atile-rich Io over 4.6 aeons. In fact, the Peale *et al.* theory suggests many such volcanoes. Furthermore, if Io had the composition of a type C3 carbonaceous chondrite, it would have an order of magnitude less volatiles, and thus the volatile depletion problem would be that much more serious. Such a composition seems more likely than a C1 composition, on theoretical grounds (*8*).

One must therefore find another volatile material to drive the volcanism observed on Io. Such a substance must be able to be recycled into the interior of Io (if volcanism spews material at the rate of 10^9 g/sec per volcano, then the whole mass of Io would have been processed ten times, given six such volcanoes). It also should be cosmochemically reasonable. Such an element is sulfur.

Hydrated calcium and magnesium sulfates make up 22 percent of typical C1 material (which translates to a sulfur content of 5.5 percent by weight for C1's), and troilite makes up 7 percent of the mass of a typical C3 composition (giving an abundance of 2.5 percent by weight for sulfur). Other heavy volatiles, such as sodium, are at least an order of magnitude less abundant. Various sulfur compounds such as SO_2 and H_2S are common constituents of terrestrial volcanoes, and these have been suggested as being present in the Ionian volcanic gas (*2*). Presumably all these volatiles could have been present in Io originally; indeed, the presence of water may have been necessary to oxidize FeS, in the presence of FeO, producing magnetite and H_2S. However, once the entire planet had been outgassed for the first time, only S_2 would remain. The destruction by solar UV of the other gases, with the subsequent loss of oxygen and hydrogen, suggests that the driving gas in Ionian volcanoes at the present time must be elemental sulfur. Finally, sulfur has been suggested as a likely surface material of Io (*2*, *9*).

At the surface temperature of Io (100 K) sulfur will be in a crystalline state with a negligible vapor pressure ($<< 10^{-9}$ bar); at lithostatic pressures deep within the interior it will be in the liquid or supercritical fluid phase. However, near the surface where gases in the rock become in contact with the surface ambient pressures, the hydrostatic rather than the lithostatic pressure confines the gas. On Io this pressure is close to that of a vacuum. Even at 1 atm, crystalline sulfur vaporizes at 444°C. Under Io conditions, it is clear that fluid sulfur in contact with magma will vaporize when the rising magma approaches the surface of the planet. The dominant molecule in the gas phase above 1000°C should be S_2; the vapor pressure of sulfur at this temperature is on the order of 1 kbar.

On eruption, S_2 gas should cool quickly and condense on the surface before destruction by solar UV can take place. Once on the surface, it could be recycled into the planet either by deep convection of the lithosphere, as suggested by Peale *et al.* (*1*), or by simple diffusion and percolation (similar to groundwater on Earth), coming in contact with rising magma at relatively shallow depths.

Such percolation will be possible once the sulfur is liquid. Assuming that the sulfur on the surface is at 100 K and that the thermal gradient is 1300 K in 18 km, as suggested by Peale *et al.* (*1*), this sulfur would have to be buried to a depth of 4 km to reach its melting temperature. Given the eruption rate of 2×10^9 g/sec as before, the entire surface of Io would be buried to this depth in less than 10 million years. The lithostatic pressure at this point is 250 bars; the vapor pressure of sulfur at 400 K is 10^{-5} bar. Thus volcanism will not occur until this liquid sulfur comes in contact with rising hot magma.

Quantitative calculations on the role of sulfur in the eruption process will depend on knowledge of the actual thermal gradient within Io and the lithospheric stresses on the surface and measurements of the number and size of the eruptions themselves. With such measurements, it should be possible to test various models of the interior and thermal structure of Io—for example, to determine the mechanical properties of the crustal material, the depth at which sulfur comes in contact with the ambient surface atmospheric pressure, and whether the upper lithosphere of Io is convecting. The ability to test such models will be important not only in understanding the interior of Io, but also in determining the strengths and weaknesses of competing modeling techniques that may be applicable to the other terrestrial planets.

GUY J. CONSOLMAGNO
Harvard-Smithsonian Center for Astrophysics, Cambridge, Massachusetts 02138

References and Notes

1. S. J. Peale, P. Cassen, R. T. Reynolds, *Science* **203**, 892 (1979).
2. The Washington *Post*, 14 March 1979; B. A. Smith *et al.*, *Science* **204**, 951 (1979); L. A. Morabito, S. P. Synnott, P. N. Kupferman, S. A. Collins, *ibid.*, p. 972.
3. F. P. Fanale, T. V. Johnson, D. L. Matson, in *Planetary Satellites*, J. A. Burns, Ed. (Univ. of Arizona Press, Tucson, 1977), pp. 379–405.
4. W. H. Smyth and M. B. McElroy, *Planet. Space Sci.* **25**, 415 (1977).
5. Y. L. Yung and M. B. McElroy, *Icarus* **30**, 97 (1977).
6. C. Ollier, *Volcanoes* (MIT Press, Cambridge, Mass., 1969); G. A. Macdonald, *Volcanoes* (Prentice-Hall, Englewood Cliffs, N.J., 1972).
7. R. Greeley, in *Volcanism of the Eastern Snake River Plain, Idaho*, R. Greeley and J. S. Kind, Eds. (National Aeronautics and Space Administration, Washington, D.C., 1977).
8. J. B. Pollack and R. T. Reynolds, *Icarus* **21**, 248 (1974); G. J. Consolmagno and J. S. Lewis, in *Planetary Satellites*, J. A. Burns, Ed. (Univ. of Arizona Press, Tucson, 1977), pp. 452–500. In brief, a body as volatile-rich as a C1 chondrite would be likely to evolve into a satellite like Europa—that is, mostly rocky but with a substantial ice crust. If Europa did evolve from C1 material, then it is likely that the original Io material, being closer to Jupiter, had less volatile elements.
9. L. A. Lebofsky, *Bull. Am. Astron. Soc.* **4**, 362 (1972); G. P. Kuiper, *Commun. Lunar Planet. Lab.* **10**, 28 (1973).
10. I thank H. Clement, C. C. Allen, S. Soter, J. C. Gradie, B. Fryxell, W. H. Smyth, and A. G. W. Cameron for helpful discussions. This work was supported by NASA grant 22-007-269.

11 April 1979; revised 31 May 1979

Samarium-Neodymium Systematics in Kimberlites and in the Minerals of Garnet Lherzolite Inclusions

Abstract. *The initial ratios of neodymium-143 to neodymium-144 in kimberlites ranging in age between 90 × 10⁶ to 1300 × 10⁶ years from South Africa, India, and the United States are different from the corresponding ratios in the minerals of peridotite inclusions in the kimberlites but are identical to the ratios in the basaltic achondrite Juvinas at the times of emplacement of the respective kimberlite pipes. This correlation between the kimberlites and Juvinas, which represents the bulk chondritic earth in rare-earth elements, strongly indicates that the kimberlite's source in the mantle is chondritic in rare-earth elements and relatively primeval in composition.*

Kimberlites are almost always found in stable continental regions and are reported from southern Africa, Siberia, North America, Brazil, India, and Australia. They most commonly occur as vertical, narrow pipelike bodies (diatremes), or as thin dikes, but rarely as sills. The diatremes may have an average diameter of 300 m at the present-day erosion level; the diatremes narrow down gradually with depth until they become indistinguishable from fissures that cut the deepest known basement structures.

Kimberlite has an inequigranular, porphyritic texture; the porphyritic texture is due to relatively large crystals of oli-

0036-8075/79/0727-0398$00.50/0

Table 1. The ^{40}K-^{40}Ar ages of two kimberlites from south India; analyst, H. Mehnert, U.S. Geological Survey, Denver.

Sample	K_2O (%)	$^{40}Ar^*$ (10^{-10} mole/g)	λ $^{40}Ar^*$	Age ($\times 10^6$ years) $\pm 2\sigma$
L-1	1.03	18.122	84.0	933 ± 37
L-2	1.28	23.414	83.7	962 ± 38

*Constants: ^{40}K $\lambda_\epsilon = 0.581 \times 10^{-10}$ year^{-1}; $\lambda_\beta = 4.963 \times 10^{-10}$ year^{-1}; $^{40}K/K = 1.157 \times 10^{-4}$.

vine, enstatite, chrome-diopside, pyrope, ilmenite, and phlogopite set in a fine-grained matrix consisting primarily of serpentine, carbonate, phlogopite, magnetite, and perovskite (*1*). Many of the large crystals are derived from the disaggregation of the many inclusions that the kimberlites incorporate from the overlying mantle during the journey from their depth of origin to the earth's surface. In view of the hybrid nature of the kimberlites, we consider, for our purpose, the carbonate-rich kimberlite matrix to represent the pristine kimberlitic liquid.

During the explosive eruption, the kimberlite accidentally incorporates a variety of mantle-derived basic and ultrabasic xenoliths. Garnet lherzolites, consisting of olivine, enstatite, garnet, and chrome-diopside are by far the most abundant inclusions. In the kimberlites of southern Africa the garnet lherzolite inclusions can be grouped into two types on the basis of mineralogy, texture, and bulk composition (*2-4*). Experimental studies of the phase equilibria indicate that the natural mineral assemblages of the first group, called granular lherzolites, have originated at depths of 100 to 150 km. The second group, called the sheared lherzolites, is believed to have come from depths of 150 to 180 km (*2, 3*). These data demonstrate that kimberlites are derived from depths of at least 180 km. No other rock type that is readily available for analysis is known to have originated at greater depths.

A study of the Sm-Nd systematics of kimberlites and their inclusions provides important information about the history and evolution of the earth's mantle. We have examined two garnet lherzolite inclusions and their host kimberlites from the Bultfontein pipe in South Africa (samples B-33 and B-101) and six other kimberlites. These six kimberlites include one from the Colorado-Wyoming border (sample Nix-2); one from each of two separate kimberlite pipes (samples L1 and L2) in south India, near Lattavaram; one from the Premier pipe in South Africa; one from the 720-m level of DeBeers mine in South Africa; and one from the Benfontein kimberlite sill, also from South Africa. One major criterion that we used in selecting these samples was to choose samples that appeared to represent best the fine-grained kimberlitic matrix material with few or no large noncognate crystals. Another important consideration was to get a maximum possible range in the age of the kimberlites from different continents. The kimberlite matrix material chosen for analysis in all the kimberlites is fine-grained, bluish gray, and consists primarily of a carbonate-silicate mixture.

The two garnet lherzolite inclusions from the Bultfontein pipe represents the two contrasting groups of inclusions found in kimberlites. Sample B-33 is a coarse-grained equigranular rock (average grain size, 5 mm) consisting of olivine, enstatite, chrome-diopside, garnet, and phlogopite. Phlogopite in this rock shows a 120° grain boundary relationship with the other minerals; this result suggests that textural and chemical equilibria have been attained. Sample B-101 represents a deformed lherzolite with large elongate crystals of olivine in a finer grained matrix consisting of garnet, enstatite, and chrome-diopside. Phlogopite is absent in this sample. Mineral separates from these two inclusions were handpicked under a binocular microscope. Clear grains without inclusions and free from any surface contamination were chosen for analysis. We selected fresh-looking kimberlite matrix material in the same way, by crushing and handpicking under a binocular microscope.

A precise knowledge of the times of emplacement of the respective kimberlite pipes is needed to calculate the initial $^{143}Nd/^{144}Nd$ ratio. Zircons from the kimberlites of the Kimberley area in South Africa all show nearly the same age (90 $\times$ 10^6 years) by the U-Pb method (*5*). The Premier pipe is the only kimberlite from South Africa that shows a Rb-Sr age of 1.2×10^9 to 1.4×10^9 years (*6*). We have chosen an age of 1.3×10^9 years for this pipe. The south Indian pipes are reported to range in age between 840×10^6 and 956×10^6 years (*7*) by the K-Ar method. Analyses of samples L-1 and L-2 gave ages of 933×10^6 and 956×10^6 years, respectively (Table 1). We chose an age of 940×10^6 years for these south Indian pipes. Sample Nix-2 has not been dated, but the adjoining Schaffer pipe, at the Colorado-Wyoming state line about 9 km north of the site of the Nix-2 pipe, has been dated by the fission track method to be $377 \pm 9 \times 10^6$ years old (*8*). We assigned an age of 370×10^6 years to the Nix-2 pipe. Thus the kimberlites chosen in this study range in age from 90×10^6 to 1300×10^6 years. Our measurements (*9, 10*) of the Sm and Nd contents and of the isotopic ratios of Nd in the minerals of the garnet lherzolite inclusions and in the host kimberlites are shown in Tables 2 and 3. Table 3 also includes the $^{143}Nd/^{144}Nd$ ratios of the bulk basaltic achondrite Juvinas at the times of the respective pipe

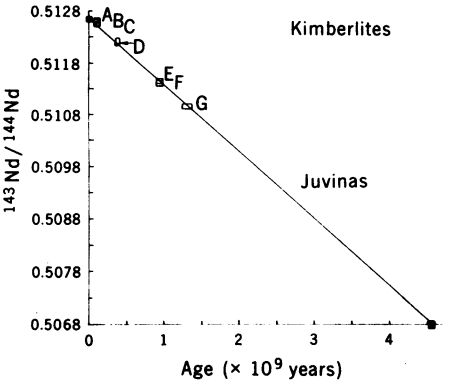

Fig. 1. A plot showing the initial $^{143}Nd/^{144}Nd$ ratios of the seven kimberlites against their age of emplacement. The line represents an independent determination of the $^{143}Nd/^{144}Nd$ evolution of the basaltic achondrite Juvinas in 4.56×10^9 years. *A*, *B*, and *C* represent the three kimberlites (Bultfontein, Benfontein, and DeBeers) from South Africa; *D* is the kimberlite from Colorado-Wyoming; *E* and *F* are the two Indian kimberlites; and *G* is the Precambrian Premier kimberlite.

Table 2. Samarium-neodymium contents and Nd isotopic compositions of the lherzolite inclusions and host kimberlite from Bultfontein; ppm, parts per million.

Mineral	Sm (ppm)	Nd (ppm)	$^{147}Sm/^{144}Nd$	$^{143}Nd/^{144}Nd$, measured*	$^{143}Nd/^{144}Nd$, initial†
		Granular lherzolite (sample B-33)			
Clinopyroxene	2.283	21.032	0.066	0.512188 ± 54	0.512145 ± 54
Garnet	1.711	4.657	0.222	0.512201 ± 32	0.512057 ± 32
Phlogopite	0.147	0.867	0.102	0.512492 ± 41	0.512425 ± 41
		Sheared lherzolite (sample B-101)			
Garnet	2.763	4.291	0.390	0.512274 ± 46	0.512045 ± 56
		Host kimberlite (sample B-109)			
Kimberlite	20.163	126.463	0.101	0.512669 ± 42	0.512610 ± 42

*Ratios are normalized to $^{150}Nd/^{144}Nd = 0.236433$. Uncertainties are 2σ mean. †The value of $^{143}Nd/^{144}Nd$, initial, is estimated by assigning a 10 percent error in the age of kimberlite and an 0.1 percent error in the measured Sm/Nd ratios.

Table 3. Samarium-neodymium contents and Nd isotopic compositions of the seven kimberlites. Pipe emplacement ages and the $^{143}Nd/^{144}Nd$ ratios in the kimberlites and in Juvinas at the times of pipe emplacement are also shown.

Kimberlite pipe	Sm (ppm)	Nd (ppm)	$^{147}Sm/^{144}Nd$	$^{143}Nd/^{144}Nd$	Age ($\times 10^6$ years)	$^{143}Nd/^{144}Nd$, initial*	$^{143}Nd/^{144}Nd$, Juvinas
				South Africa			
Bultfontein	20.163	126.463	0.1010	0.512669 ± 42	90	0.512610 ± 42	0.512522 ± 40
Benfontein (carbonatitic)	28.243	423.495	0.0695	0.512625 ± 32	90	0.512584 ± 32	0.512522 ± 40
DeBeers mine	29.24	225.39	0.0784	0.512632 ± 30	90	0.512585 ± 30	0.512522 ± 40
Premier	3.791	24.555	0.0932	0.511752 ± 27	1300	0.510956 ± 82	0.510983 ± 40
				South India			
L-1	17.254	119.353	0.0874	0.511987 ± 37	940	0.511448 ± 66	0.511442 ± 40
L-2	9.205	69.551	0.0800	0.511906 ± 30	940	0.511413 ± 65	0.511442 ± 40
				Colorado-Wyoming			
Nix-2	12.642	116.305	0.0657	0.512369 ± 19	377	0.512207 ± 19	0.512158 ± 40

*See Table 1.

emplacements. These ratios have been calculated (*11*) from the measured Sm/Nd and $^{143}Nd/^{144}Nd$ ratios of Juvinas (4.56×10^9 years old) by Lugmair *et al.* (*12*) and by Nakamura *et al.* (*9*). Table 3 shows that the kimberlites have variable patterns of light rare-earth element (REE) enrichment compared to chondrites but have low and fairly constant Sm/Nd ratios. The Benfontein carbonatitic kimberlite shows the highest light REE enrichment among all the kimberlites. We consider the variable REE patterns in the kimberlites to be due to variable carbonate-silicate ratios in the matrix materials analyzed. For example, the Premier and Benfontein samples have the highest and lowest amounts of silicate materials, respectively.

In the minerals of garnet lherzolites, the Sm and Nd contents are highest in the clinopyroxene, intermediate in the garnet, and lowest in the phlogopite (Table 2). The initial $^{143}Nd/^{144}Nd$ ratios (calculated back to the time of pipe emplacement) of garnets and of the clinopyroxene are identical within the precision of the analyses but differ from the same ratios in phlogopite and in the host kimberlite. The $^{143}Nd/^{144}Nd$ ratio of the phlogopite is intermediate between that of the host kimberlite and that of pyroxene and garnets.

The fact that the initial Nd isotopic compositions of garnets and clinopyroxene, in granular and sheared lherzolites, are identical but different from that of the host kimberlite (which is derived from a deeper level in the mantle than the lherzolites) has important implications. The above relationship reflects local isotopic homogeneities as well as vertical heterogeneity within the subcontinental mantle beneath South Africa. The lower initial $^{143}Nd/^{144}Nd$ values in the constituent minerals of the lherzolites compared with the kimberlite strongly indicate that the shallower mantle, represented by these xenoliths, has a lower Sm/Nd ratio and hence a pattern of light REE enrichment similar to that of alkalic basalts. The isotopic equilibration of coexisting garnet and clinopyroxene in the same sample lends credibility to the fundamental assumption of chemical equilibrium (*2*) in the estimation of temperatures and pressures of equilibration of the inclusions on the basis of major element partitioning. We regard the different Nd isotopic composition of the phlogopite (in sample B-33) from the coexisting clinopyroxene and garnet as due to contamination from the host kimberlite, in view of the low Nd content of the phlogopite and its intermediate isotopic composition between the kimberlite and the other minerals in the specimen. Thus, in general, the Nd isotopic data support the general conclusion from the petrologic data (*2, 3*) that the inclusions do not bear a cognate relationship with their host kimberlite. In other words, the kimberlites are derived from a different stratum (much deeper) in the mantle where the Sm/Nd ratio is larger than in the stratum from which the inclusions are derived.

Table 3 and Fig. 1 demonstrate that the initial $^{143}Nd/^{144}Nd$ ratios of the six kimberlites are identical to those of the basaltic achondrite Juvinas at the time of the respective pipe emplacement during a period of 90×10^6 to 1300×10^6 years before the present. Juvinas is a eucrite-meteorite (*13*) that gave a crystallization age of 4.56×10^9 years by the Sm-Nd method (*14*), and it has a Sm/Nd ratio very close to the chondritic ratio (*15*). The range of relative concentrations of the REE is nearly the same for both achondrites and chondrites (*16*), but there is a marked enrichment of the absolute abundances of the REE in the achondrites. Juvinas, for example, shows approximately the chondritic REE pattern—the absolute abundances being eight times that found in the chondrites (*17*). Because of its age, the same as that of the earth, and because of its chondritic Sm/Nd ratio, Juvinas can thus be used to represent the "chondritic bulk earth" (*12, 18*). Here, we use the best estimate for the present-day $^{143}Nd/^{144}Nd$ ratio of bulk Juvinas to be 0.512636 ± 40 with an initial value of 0.5068 at a time 4.56×10^9 years before the present. For the $^{147}Sm/^{146}Nd$ ratio we use 0.1936 (*9, 12*).

The most significant conclusion that emerges from our analysis of the seven kimberlites is that kimberlites are derived, in space and time, from a relatively undifferentiated, primeval, and unique mantle reservoir with an identical chondritic signature in Sm/Nd and $^{143}Nd/^{144}Nd$ ratios. The fact that the minerals of the xenoliths in kimberlites have a different Nd isotopic signature indicates a vertically complex and heterogeneous mantle beneath the continents of South Africa, India, and the United States. However, the identical chondritic Sm/Nd ratio and the chondritic Nd isotopic composition of the kimberlite's source in the mantle indicate a uniform mantle layer beneath these continents at depths below 200 km, the minimum estimated depth of derivation of kimberlitic liquid.

ASISH R. BASU*
Department of Chemistry and Geochemistry, Colorado School of Mines, Golden 80401
MITSUNOBU TATSUMOTO
Branch of Isotope Geology, U.S. Geological Survey, Denver 80225

References and Notes

1. J. B. Dawson, *Earth-Sci. Rev.* **7**, 187 (1971).
2. F. R. Boyd, *Geochim. Cosmochim. Acta* **37**, 2533 (1973).
3. I. D. MacGregor and A. R. Basu, *Science* **185**, 1007 (1974).
4. A. M. Boullier and A. Nicolas, *Phys. Chem. Earth* **9**, 467 (1974).

5. G. L. Davis, T. E. Krogh, A. J. Erlank, *Carnegie Inst. Washington Yearb.* **75**, 821 (1976).
6. D. R. Barrett and H. L. Allsopp, paper presented at the First International Kimberlite Conference, University of Cape Town, Cape Town, South Africa, 1973.
7. D. K. Paul, D. C. Rex, P. G. Harris, *Geol. Soc. Am. Bull.* **86**, 364 (1975).
8. C. W. Naeser and M. E. McCallum, paper presented at the Second International Kimberlite Conference, Santa Fe, N.M., 1977.
9. N. Nakamura, M. Tatsumoto, P. D. Nunes, D. M. Unruh, A. P. Schwale, T. R. Wildeman, *Proc. 7th Lunar Sci. Conf.* (1976), p. 2309.
10. Over a period of 3 years, three different operators have analyzed the National Bureau of Standards Nd shelf standard in our laboratory with identical results. Errors in the estimation of the Sm and Nd contents are 0.1 percent or less for the kimberlites and slightly higher (up to 0.3 percent) for the minerals in the xenoliths. The Sm and Nd blanks were within the range reported in (9).
11. The initial $^{143}Nd/^{144}Nd$ ratio, I, at a time (T) is calculated from the equation:

$$I = \left(\frac{^{143}Nd}{^{144}Nd}\right)_{measured} - \left(\frac{^{147}Sm}{^{144}Nd}\right)_{measured} (e^{\lambda T} - 1)$$

where the decay constant $\lambda = 6.54 \times 10^{-12}$ year^{-1}.
12. G. W. Lugmair, N. B. Scheinin, K. Marti, *Proc. 6th Lunar Sci. Conf.* (1975), p. 1419.
13. M. B. Duke and L. T. Silver, *Geochim. Cosmochim. Acta* **31**, 1637 (1967).
14. G. W. Lugmair *et al.*, *Proc 7th Lunar Sci. Conf.* (1976), p. 2009.
15. A. Masuda, N. Nakamura, T. Tanaka, *Geochim. Cosmochim. Acta* **37**, 239 (1973); N. Nakamura, *ibid.* **38**, 757 (1974).
16. R. A. Schmitt, R. H. Smith, J. E. Lasch, A. W. Mosen, D. A. Olehy, J. Vasilevskis, *ibid.* **27**, 577 (1963).
17. C. C. Schnetzler and J. A. Philpotts, in *Meteorite Research*, P. M. Millman, Ed. (Reidel, Dordrecht, 1969), p. 206.
18. D. J. DePaolo and G. J. Wasserburg, *Geophys. Res. Lett.* **3**, 249 (1976).
19. We thank I. D. MacGregor for providing many of the samples used in this study. We thank Drs. F. R. Boyd, D. H. Eggler, and C. H. Smith, who also provided kimberlite samples. We are grateful to Drs. F. R. Boyd, D. H. Eggler, S. R. Hart, A. W. Hoffman, C. H. Langmuir, I. D. MacGregor, Z. E. Peterman, and H. S. Yoder for reviewing the manuscript. This research was supported by NASA interagency transfer order T-2407 A.
* Present address: Department of Geological Sciences, University of Rochester, Rochester, N.Y. 14627.

8 January 1979

Flash X-ray Microscopy

Abstract. *Soft x-ray contact microscopy, utilizing single-shot exposures of ~ 60 nanoseconds duration in polymethyl methacrylate, has been realized with a resolution of 300 angstroms. The radiation spectrum is intense in the "window" between 23 and 44 angstroms where water is transparent compared to biological materials, and therefore permits viewing of wet samples.*

Recent interest in the x-ray microscopy of biological objects has been fostered by the high-resolution (≤ 100 Å) capabilities of contact microscopy in which x-ray resists are used in combination with the comparatively short exposure times (minutes) realizable with synchrotron sources (*1*). Development of synchrotron sources to provide intense soft x-ray flux is well under way (*2*). The operating region for soft x-ray microscopy has been defined and comparisons made with competitive microscopies, such as electron microscopy (*3*).

The present work with a new soft x-ray source (*4*) extends the high-resolution x-ray microscopy technique in several important respects. Exposure times have been drastically reduced: single-shot flash x-ray exposures of ~ 60 nsec duration have been obtained. Because of the charge states of the emitting element (C^{4+} and C^{5+}), the dominant x-ray emission wavelength is optimum for high-resolution work (*1*). Moreover, emission is not restricted to a single wavelength, but contains a band that has been found to be of advantage in minimizing diffraction effects as well as facilitating high contrast in thin regions while avoiding excess opacity in dense regions (*5*). Also, the shifted line emission, as compared to solid target emission, occurs within the "window" region for wet-sample viewing; that is, within the wavelength region for which water is transparent in comparison with biological materials. Therefore, x-ray microscopy of living organisms may be realizable, one possibility being the microscopic study of radiation damage to cellular structures. The source spectrum (*4*) contains very little hard x-ray emission. Hard components have been found to be detrimental to resolution as well as damaging to the specimen (*1*). The small source size (*4*) (~ 200 μm) eliminates penumbral blurring. Finally, the x-ray source is very compact and inexpensive.

The work reported here is based on utilization of a novel x-ray tube (see Figs. 1A and 2A). The tube comprises a discharge capillary for producing, by erosion of several monolayers of the capillary wall, a dense, high-temperature plasma. Typically, for microscopy, a polyethylene capillary is employed with graphite electrodes. A carbon plasma with an electron density of ~ 3×10^{19} cm^{-3} and a temperature of 35 to 40 eV is produced, the dominant charge state being C^{4+}. In addition, the tube contains a rod cathode for launching an intense electron beam (5 to 10 kA at 30 to 100 kV) into the plasma to enhance the soft x-ray emission. A special diode configuration was used to obtain clean operation of the beam-plasma system. The entire tube can be self-triggering or can rely on a single trigger electrode if a predetermined pulse time is desirable. Both the plasma discharge and the electron beam are driven by simple capacitance

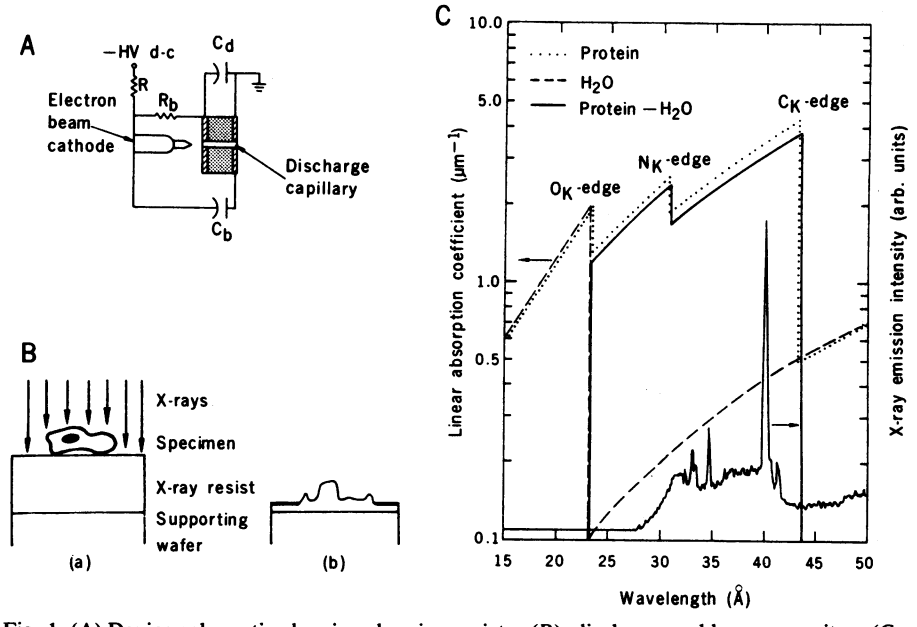

Fig. 1. (A) Device schematic showing charging resistor (R), discharge and beam capacitors (C_d and C_b, respectively), beam isolation resistor (R_b), and beam cathode and discharge capillary positioning. (B) Irradiation of the x-ray resist through the specimen (a), and the replica after development of the resist (b). (C) Superposition of densitometer trace of x-ray output as a function of wavelength with the absorption characteristics of protein, water, and protein minus water. Strong x-ray emission is seen to occur in the water window between 23 and 44 Å, allowing wet-sample viewing.

0036-8075/79/0727-0401$00.50/0